

Quantifying the Properties of Nonproductive Attempts at Thermally Activated Energy-Barrier Crossing through Direct Observation

Aaron Lyons,¹ Anita Devi,¹ Noel Q. Hoffer,¹ and Michael T. Woodside^{1,2,3,*}

¹*Department of Physics, University of Alberta, Edmonton, Alberta T6G 2E1, Canada*

²*Centre for Prions and Protein Folding Diseases, University of Alberta, Edmonton Alberta T6G 2E1, Canada*

³*Li Ka Shing Institute of Virology, University of Alberta, Edmonton, Alberta T6G 2E1, Canada*



(Received 26 June 2023; revised 27 October 2023; accepted 17 November 2023; published 14 February 2024)

Thermally activated energy-barrier crossing is ubiquitous in physical, chemical, and biological processes. Most barrier-crossing attempts have insufficient energy to overcome the barrier; hence, productive transition paths that successfully cross the barrier are very rare compared to nonproductive fluctuations that enter the barrier region but return without crossing it. Recent experimental advances have yielded important insights into transition paths, but nonproductive attempts remain little studied experimentally or theoretically, even though they can reveal information about parts of the reaction energy landscape not visited during transition paths. Observing the diffusive dynamics of a bead hopping between bistable optical traps as a model system, we measured the duration, maximum position along the reaction coordinate, and occupancy statistics of unsuccessful crossing attempts. Experimental results agreed quantitatively with expectations of an analytical framework we derived from committor theory. Applying these analyses to a more complex example, DNA hairpin folding under tension, we found that some properties differed from those of transition paths, such as the asymmetric occupancies for folding and unfolding attempts, whereas others were similar, such as the diffusion coefficient reflecting landscape roughness. These results show how nonproductive crossing attempts can be detected and analyzed rigorously, enabling characterization of the full dynamics within the transition region.

DOI: [10.1103/PhysRevX.14.011017](https://doi.org/10.1103/PhysRevX.14.011017)

Subject Areas: Biological Physics, Chemical Physics

I. INTRODUCTION

A vast range of processes across the physical and life sciences involve thermally activated crossing of an energy barrier, from chemical and enzymatic reactions to transport processes in condensed matter, crystallization, and protein folding. As first recognized by Arrhenius over 130 years ago and later codified more completely by Kramers [1], successful barrier-crossing events are rare: The great majority of attempts are unsuccessful, entering the barrier region but failing to cross all the way over (Fig. 1). Owing to the obvious importance of the attempts that succeed at crossing the barrier, almost all efforts at characterizing reaction trajectories have focused on such productive “transition paths” (Fig. 1, blue). Transition paths pose a particular challenge technically because they are both rare and brief, but they have been studied computationally using methods for sampling rare events [2] and, more recently,

through direct observation in experiments [3]. Such studies have led to important insights into properties of transition paths such as their duration, occupancy, shape, and velocity profile [4–10]. In contrast, however, the properties of the nonproductive fluctuations that are associated with unsuccessful crossing attempts (Fig. 1, red) remain almost completely uncharacterized, as they have been little studied computationally, experimentally, or theoretically.

Naively, it might seem that there is not much to learn from studying unsuccessful attempts, precisely because they are nonproductive. However, nonproductive fluctuations typically explore more of the reaction phase space than do productive transition paths, and they may thereby provide new information—not accessible from transition paths—about the parts of the reaction-defining energy landscape through which transition paths do not pass (see Fig. S1 in Supplemental Material [11]). In some cases, such “off-pathway” behavior may in fact be crucially important. For example, protein folding reactions often involve nonproductive fluctuations into incorrect (“misfolded”) conformations [12–14]; given that misfolded proteins can sometimes cause disease [15], characterizing the properties of unsuccessful folding attempts may provide key insights into pathogenic misfolding mechanisms. More generally, studying nonproductive fluctuations in

*Corresponding author: michael.woodside@ualberta.ca

Published by the American Physical Society under the terms of the [Creative Commons Attribution 4.0 International license](https://creativecommons.org/licenses/by/4.0/). Further distribution of this work must maintain attribution to the author(s) and the published article's title, journal citation, and DOI.

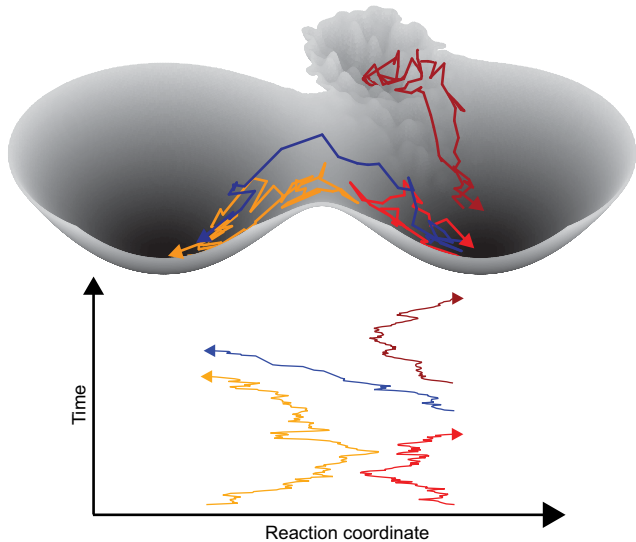


FIG. 1. Transition paths and nonproductive fluctuations. Transition paths (blue) cross from one well to the other. Unsuccessful attempts at forward (red) and reverse (orange) reactions fluctuate into the barrier region but do not cross it. Some nonproductive fluctuations (dark red) may sample parts of the energy landscape not explored in transition paths but possibly having different properties (e.g., greater roughness).

addition to transition paths allows for the most complete characterization possible of the dynamics within the transition region, for any reaction.

Here, we aim to quantify the properties of nonproductive attempts at thermally activated crossing of an energy barrier through direct observation and to develop a framework for analyzing key observables. Studying first the diffusive hopping of a bead between bistable optical traps as a model system for single-barrier reactions [16,17], we monitor the trajectory of the bead as it fluctuates thermally within the traps to identify both productive transition paths crossing from one trap to the other and nonproductive fluctuations into the barrier region that return to the same trap from which they start. We characterize the unsuccessful attempts through properties such as their duration, occupancy distribution, and maximum distance reached along the reaction coordinate. Deriving analytical expressions for these properties based on committor theory, we find quantitative agreement with observations, validating the analysis approach. Finally, we apply this approach to a more complex system: unfolding of a DNA hairpin held under tension in optical tweezers [18]. We find that the occupancy distributions for nonproductive fluctuations of the hairpin differ from those of transition paths by being asymmetric, but the conformational diffusion coefficient is the same as for transition paths. This work shows how nonproductive barrier-crossing attempts can be measured directly and their properties analyzed to obtain a more complete understanding of the dynamics of thermally activated reactions.

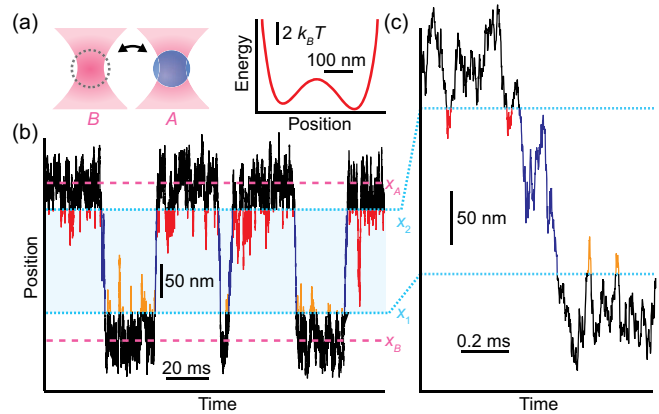


FIG. 2. Bead hopping in bistable traps. (a) Left: measurement schematic. A bead hops between potential wells defined by optical traps A and B . Right: energy landscape governing hopping. (b) Hopping trajectory (cyan: barrier region bounded by x_1 and x_2). (c) Trajectory segment showing transition path (blue) and unsuccessful attempts (forward crossing attempts: red; reverse crossing attempts: orange).

II. RESULTS

A. Bead hopping in a bistable potential

To study thermally activated barrier crossing in a controlled reaction with a well-characterized energy barrier, we used diffusive hopping of a micron-scale bead between bistable optical traps [Fig. 2(a), left]. Similar to previous work validating Kramers' classic theory of reaction rates [16] and theories of transition paths [17], this model system is ideal for testing theoretical descriptions as it involves purely Brownian diffusion of a sphere within a known potential. A single polystyrene bead of radius 410 nm was held in a pair of traps separated by $0.23 \mu\text{m}$. The trap stiffness (roughly 0.005 pN/nm) was set to obtain a barrier height of about $2.5 k_B T$, leading to rates on the order of a few crossings per second. The bead dynamics were measured at 1-MHz bandwidth from light scattered onto a quadrant photodiode to generate trajectories of position as a function of time [Fig. 2(b)]. Because the bead motions were driven entirely by thermal fluctuations, the energy potential created by the traps, $U(x)$, could be quantified (to within a constant) from the bead position distribution, $p(x)$, via $\beta U(x) = -\ln[p(x)]$, where β is the inverse thermal energy [Fig. 2(a), right].

The bead trajectories contained multiple transitions where the bead hopped between the two traps, A and B (centers of the traps denoted by x_A and x_B), as well as a great many nonproductive fluctuations reaching part of the way into the barrier region between the traps. Defining the barrier region as the middle two-thirds of the distance between the two traps, bounded by x_1 and x_2 [Fig. 2(b), cyan], we identified those parts of the trajectories passing from x_1 to x_2 without first recrossing x_1 (or vice versa) as transition paths, and all those parts looping from x_1 towards

x_2 but returning to x_1 before crossing x_2 (or vice versa) as nonproductive crossing attempts. Zooming in on a short segment of the trajectory [Fig. 2(c)], transition paths are shown in blue, whereas nonproductive fluctuations are shown in red (attempts to cross from A to B , hereafter denoted the forward reaction) or orange (attempts to cross from B to A , hereafter denoted the reverse reaction).

B. Position distributions for nonproductive fluctuations

We first examined the occupancy distributions for nonproductive fluctuations in the forward and reverse directions, respectively $p(x|\text{NPF}_F)$ and $p(x|\text{NPF}_R)$ [Fig. 3(a)]. These distributions are constructed by compiling all positions adopted by nonproductive fluctuations originating from either state, and they reflect the probability of finding the bead at x given that it is undergoing a barrier crossing attempt. As expected, $p(x|\text{NPF}_F)$ [Fig. 3(a), red] dropped off rapidly as the bead moved away from A and towards B because higher-energy fluctuations that could reach far into the barrier region were much rarer than smaller, lower-energy fluctuations; the same situation held for $p(x|\text{NPF}_R)$ but in the opposite direction [Fig. 3(a), orange].

To compare the observations to theoretical expectations, we derived the equilibrium distributions for forward

and reverse fluctuations under the assumption of one-dimensional (1D) diffusion. Following previous work [19], we first used the Smoluchowski equation to find the probability distribution for diffusive trajectories that start at position x_0 in the transition region ($x_1 < x_0 < x_2$) and are absorbed at either of the transition-region boundaries. Taking the limit as x_0 approaches x_1 or x_2 then yields the distribution of points in the transition region for all trajectories originating, respectively, from the product or reactant state, which can be separated into those that terminate at x_1 or x_2 by multiplying them by one of the committor functions $\Phi_F(x)$ or $\Phi_R(x)$, $\Phi_F(x|x_1, x_2) = \int_x^{x_2} \exp[\beta U(x)] / \int_{x_1}^{x_2} \exp[\beta U(x)]$ and $\Phi_R = 1 - \Phi_F$, where $\Phi_F(x)$ describes the probability that a diffusive trajectory starting at x reaches x_1 before x_2 (i.e., reaches the product state before the reactant state) and $\Phi_R(x)$ the reverse. Multiplying the distribution for trajectories originating from one state by the probability that they reach the opposite state first before returning yields the distribution for transition paths, as derived previously [19] and validated experimentally [20,21]. Conversely, multiplying the distribution for trajectories originating from one state by the probability that they return to that state before reaching the opposite state yields the position distribution for unsuccessful forward or reverse reaction attempts:

$$\begin{aligned}
 p(x|\text{NPF}_F) &\propto \exp[-\beta U(x)] [\Phi_R(x|x_1, x_2)]^2, \\
 p(x|\text{NPF}_R) &\propto \exp[-\beta U(x)] [\Phi_F(x|x_1, x_2)]^2.
 \end{aligned} \quad (1)$$

To test if the observed position distributions matched theoretical expectations, we used the potential $U(x)$ calculated from the distribution of all bead positions to determine the distributions of nonproductive fluctuations via Eq. (1). We found excellent quantitative agreement with the observations for both forward and reverse reactions [Fig. 3(a), blue]; note that this comparison is not a fit but rather a parameter-free comparison between experiment and theory. Because the double-well potential was close to symmetric [Fig. 2(a), inset], $p(x|\text{NPF}_F)$ and $p(x|\text{NPF}_R)$ were close to mirror images of each other.

C. Maximum extent of nonproductive fluctuations

Next, to quantify the size of the nonproductive fluctuations, we measured the maximum distance each fluctuation reached into the barrier region [Fig. 3(b), inset]. The distributions of maximum distances, $p(x_{\max}|\text{NPF}_F)$ and $p(x_{\max}|\text{NPF}_R)$, respectively, for forward and reverse reactions, again showed a sharp drop as the maximum distance moved away from the boundary towards the other side of the barrier region [Fig. 3(b), red: $p(x_{\max}|\text{NPF}_F)$, orange: $p(x_{\max}|\text{NPF}_R)$].

To find theoretical predictions for these distributions, we first derived expressions for the rate at which

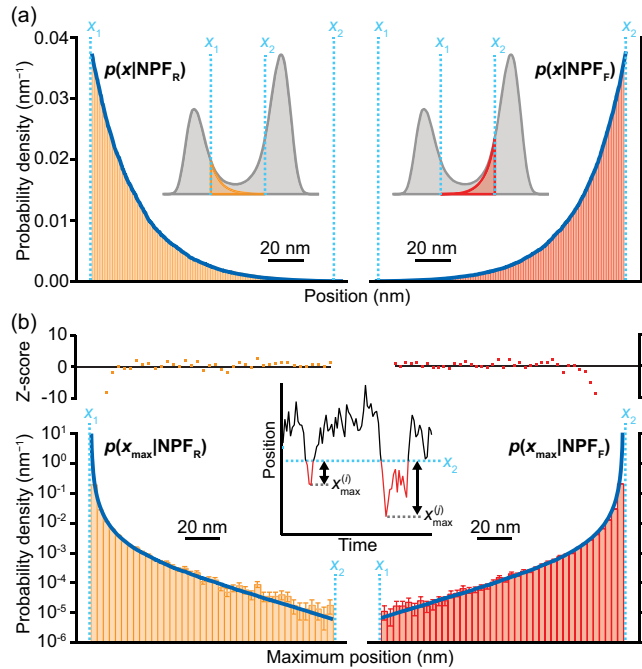


FIG. 3. Position distribution and maximum extent of nonproductive fluctuations. (a) Position distributions $p(x|\text{NPF}_F)$ (red) and $p(x|\text{NPF}_R)$ (orange), with theoretical expectations from Eq. (1) (blue). Insets: predicted distributions compared to the total occupancy distribution (gray). (b) Distributions of maximum distances $p(x_{\max}|\text{NPF}_F)$ (red) and $p(x_{\max}|\text{NPF}_R)$ (orange), with fits to Eq. (5) (blue) and residual Z-scores. Inset: definition of x_{\max} .

nonproductive fluctuations reaching x_{\max} occur. The rate for transition paths was previously reported as [22]

$$k(\text{TP}_F) = k(\text{TP}_R) = \frac{D}{\int_{-\infty}^{\infty} \exp[-\beta U(x)] dx} \frac{1}{\int_{x_1}^{x_2} \exp[\beta U(x)] dx}. \quad (2)$$

These rates change as x_1 or x_2 are moved, owing to reclassification of transition paths as nonproductive fluctuations or vice versa—for example, barrier crossing attempts that nearly reach the opposite state before returning may become transition paths if the opposite state boundary is brought closer to the center of the transition region. For a small change Δx in boundary location, the change in the transition-path rate can therefore be attributed to the rate at which nonproductive fluctuations reaching their maximum position within the interval Δx occur. The rate densities for unsuccessful forward or reverse reaction attempts reaching their maximum extent at x_{\max} , $k(x_{\max}|\text{NPF}_{F/R})$, are then given by the derivative of Eq. (2) with respect to x_1 or x_2 , respectively,

$$k(x_{\max}|\text{NPF}_F) = \frac{D}{\int_{-\infty}^{\infty} \exp[-\beta U(x)] dx} \frac{\exp(\beta U(x_{\max}))}{\int_{x_{\max}}^{x_2} \exp[\beta U(x)] dx}. \quad (3)$$

$$k(x_{\max}|\text{NPF}_R) = \frac{D}{\int_{-\infty}^{\infty} \exp[-\beta U(x)] dx} \frac{\exp(\beta U(x_{\max}))}{\int_{x_1}^{x_{\max}} \exp[\beta U(x)] dx}. \quad (4)$$

In principle, normalization by integrating the rate density over x_{\max} from x_1 to x_2 yields $p(x_{\max}|\text{NPF}_{F/R})$. In practice, however, the analysis is complicated by a singularity: The distributions are singular at the boundaries [$x_{\max} = x_2$ for $p(x_{\max}|\text{NPF}_F)$ and x_1 for $p(x_{\max}|\text{NPF}_R)$] because, in pure 1D diffusion, there are an infinite number of crossings that go only an infinitesimal distance into the barrier region. Experimentally, the finite measurement resolution in time and space filters out such short fluctuations, as recognized previously [23], effectively flattening the distribution near the boundaries. To compare our observations to theory, we therefore truncated the distribution near the boundary before fitting to the expressions derived from Eqs. (3) and (4):

$$p(x_{\max}|\text{NPF}_F) \propto \exp[\beta U(x_{\max})] / \left(\int_{x_{\max}}^{x_2} \exp[\beta U(x)] dx \right)^2, \quad (5)$$

with a corresponding expression for $p(x_{\max}|\text{NPF}_R)$. Treating the normalization constant as a free parameter, we found excellent agreement with the data [Fig. 3(c), blue] if we excluded the positions within about 10–20 nm of the

boundary (Fig. S2 in Ref. [11]), suggesting that the finite sampling effects were significant only within that region.

D. Average nonproductive fluctuation durations

Finally, we examined the duration of the nonproductive fluctuations, measuring directly from the trajectories the time spent within the barrier region during such fluctuations [Fig. 4(a), right inset]. The average duration is theoretically expected to be zero because of the infinite number of infinitesimal fluctuations in purely diffusive motion, but it becomes finite owing to experimental resolution limits [23] and the crossover to ballistic transport at short timescales [24]. The observed distribution of fluctuation times dropped rapidly but had a long tail [Fig. 4(a)]. Focusing on the average duration as a function of the maximum distance reached, $\tau(x_{\max})$, which should provide a good estimate for those fluctuations large

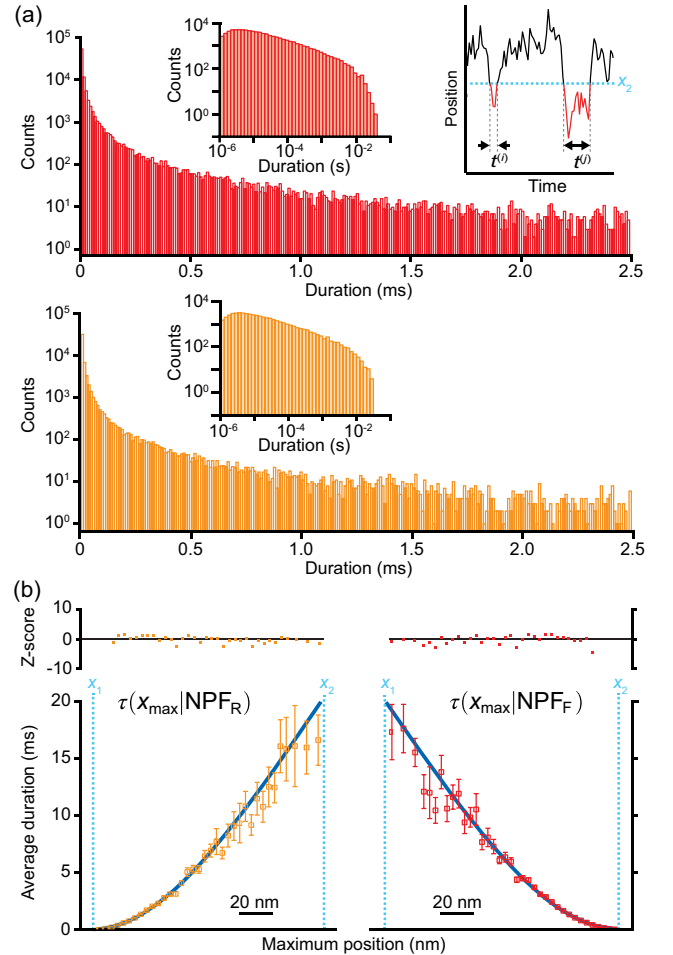


FIG. 4. Duration of nonproductive fluctuations. (a) Duration of unsuccessful forward (red) and reverse (orange) attempts. Right inset: definition of attempt duration. (b) Average duration as a function of maximum position for forward (red) and reverse (orange) attempts, with fits to Eq. (7) (blue) and residual Z-scores.

enough to avoid experimental filtering effects, we found that it rose superlinearly as the maximum extent of the fluctuation increased [Fig. 4(b), red: $\tau(x_{\max}|\text{NPF}_F)$; orange: $\tau(x_{\max}|\text{NPF}_R)$].

To derive theoretical predictions for $\tau(x_{\max}|\text{NPF}_F)$ and $\tau(x_{\max}|\text{NPF}_R)$, we used the fact that the average duration of an event is the fraction of time spent on those events divided by the rate at which they occur [19,25]. The proportion of time spent on each reaction attempt is given by the integral of Eq. (1) over the barrier region (normalized to the expected sum of all occupancies):

$$P(\text{NPF}_F) = \frac{\int_{x_1}^{x_2} \exp[-\beta U(x)] [\Phi_R(x|x_1, x_2)]^2 dx}{\int_{-\infty}^{\infty} \exp[-\beta U(x)] dx}, \quad (6)$$

with a corresponding expression for $P(\text{NPF}_R)$. Differentiating with respect to the relevant boundary position (as for the rate densities above) and dividing by the rate densities then yields the average duration for nonproductive forward fluctuations reaching the maximum extent x_{\max} :

$$\begin{aligned} \tau(x_{\max}|\text{NPF}_F) &= \frac{2}{D} \int_{x_{\max}}^{x_2} \exp[-\beta U(x)] \Phi_F(x|x_{\max}, x_2) \\ &\quad \times \Phi_R(x|x_{\max}, x_2) dx \left[\int_{x_{\max}}^{x_2} \exp[\beta U(x)] dx \right], \end{aligned} \quad (7)$$

again with a corresponding expression for reverse fluctuations (swapping x_1 for x_{\max} and x_{\max} for x_2). Finally, to account for the experimental overestimation of path times owing to finite sampling effects [23], we added a linear offset term t_0 .

Comparing to the data, we found very good agreement with Eq. (7) [Fig. 3(d), blue] when excluding data within about 10–20 nm of the boundary (Fig. S3 in Ref. [11]). This range is the same as that excluded in the analysis of $p(x_{\max}|\text{NPF})$, suggesting that the sensitivity to finite-sampling effects is similar for $\tau(x_{\max})$. The offset term t_0 was about 50–100 μs , suggesting that the overestimation of average durations due to unobserved barrier recrossing was only about 1% of the average transition path time for this system.

Notably, the fit of $\tau(x_{\max})$ to Eq. (7) returns the diffusion coefficient for dynamics in nonproductive fluctuations, D . Here, we found $D = 2.9 \pm 0.1 \times 10^5 \text{ nm}^2/\text{s}$ from the forward attempts and $2.8 \pm 0.1 \times 10^5 \text{ nm}^2/\text{s}$ from the reverse attempts. For motion of a spherical bead of radius R through fluid of viscosity η , we would expect $D = k_B T / 6\pi\eta R = 5.5 \times 10^5 \text{ nm}^2/\text{s}$ under the conditions of our measurements. The observed value is lower, presumably owing to spatial inhomogeneities in the laser beam intensity introduced by the acousto-optic deflectors used for position and stiffness control [26] that generate roughness in the

potential landscape, thereby reducing D [27]; the reduction of around twofold in D observed here suggests that this roughness is approximately $0.6 k_B T$. To test if the value of D obtained from this analysis is reasonable, we compared it to the value found from the average transition path time τ_{TP} using exact calculations based on the measured landscape [19]. The observed value $\tau_{\text{TP}} = 9.6 \pm 0.2 \text{ ms}$ yielded $D = 2.91 \pm 0.07 \times 10^5 \text{ nm}^2/\text{s}$ for transition paths, in excellent agreement with the results from nonproductive attempts.

E. Application to DNA hairpin folding

Having demonstrated a framework for characterizing the properties of nonproductive fluctuations in a model system, we next applied it to a more complex reaction: the folding of a biological macromolecule. Folding reactions are of significant importance in the life sciences, as biomolecules must self-assemble into the correct structures in order to function properly. We focused on the folding of a DNA hairpin, hairpin 30R50/T4 [28], whose energy-landscape and transition-path properties have been studied extensively [5,6,8,10,18,29–31]. The hairpin was attached to kilobase-long handles of double-stranded DNA bound at each end to beads held in independently controlled optical traps [Fig. 5(a)]. A constant force was applied to the hairpin by the traps with a passive force clamp [32], such that the hairpin unfolded and refolded reversibly in equilibrium. Measurements of the end-to-end extension of the DNA construct generated trajectories that were qualitatively similar to those seen for the hopping bead [Fig. 5(b)] but now encoding the dynamics of a much richer system. Identifying the boundaries of the barrier region as for the bead-hopping measurement, individual nonproductive attempts at folding (forward reaction) and unfolding (reverse reaction), as well as productive transition paths, were then identified directly from the trajectories [Fig. 5(c), red: folding attempts; orange: unfolding attempts; blue: transition paths].

As with bead hopping, nonproductive fluctuations dominated the dynamics in the barrier region, but here they showed different spatial distributions and attempt frequencies for folding versus unfolding [Fig. 5(d) inset, red: folding attempts; orange: unfolding attempts]. This asymmetry reflected the asymmetry of the hairpin folding landscape, where the barrier was much closer to the unfolded state than the folded state [18]. However, the presence of the handles and beads—whose own fluctuations, independent of the hairpin dynamics, also contributed to the fluctuations observed in the trajectories—complicated the picture. To assess the contributions from the beads and handles, we analyzed $p(x_{\max})$ (the distribution of maximum fluctuation extent) from a reference construct containing the same handles but no hairpin (Fig. S4 in Ref. [11]) and then compared our results to the results from the hairpin construct [Fig. 5(e), red: folding attempts; orange: unfolding attempts; gray: bead and handle fluctuations]. The bead and handle

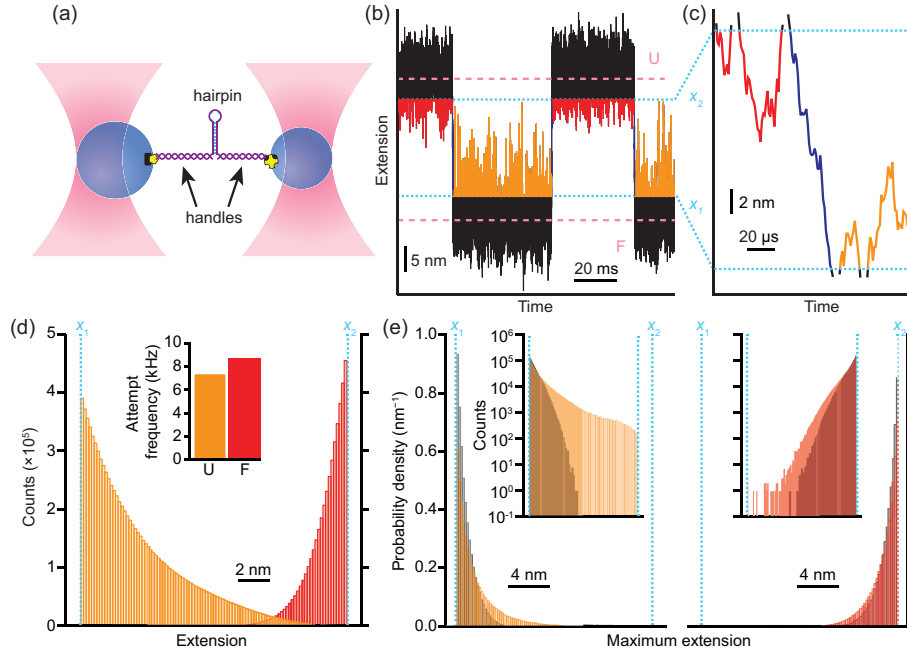


FIG. 5. Nonproductive fluctuations in DNA hairpin folding at constant force. (a) Schematic of measurement: force applied to a DNA hairpin tethered between trapped beads causes the hairpin to unfold and refold reversibly. (b) Extension trajectory showing hopping between unfolded (U) and folded (F) states. (c) Examples of folding attempts (red), unfolding attempts (orange), and a transition path (blue). (d) Occupancy distributions for folding (red) and unfolding (orange) attempts, which are not symmetric. Inset: attempt frequencies for folding (red) and unfolding (orange). (e) Maximum extension distributions for folding (red) and unfolding (orange), with comparable distributions for bead and handle fluctuations only (gray).

fluctuations were significant close to the boundaries x_1 and x_2 , but hairpin fluctuations dominated beyond around 4 nm into the barrier region, confirming that we were indeed observing unsuccessful folding and unfolding attempts in those parts of the barrier. Nevertheless, the contributions of the bead and handle fluctuations led to relatively poor agreement between the observed occupancy distributions $p(x|NPF_F)$ and $p(x|NPF_U)$ (respectively, for folding and unfolding) and the results expected from the measured landscape (Fig. S5 in Ref. [11]).

These results showed that nonproductive attempts could indeed be detected in constant-force measurements. However, owing to low effective trap stiffness, the time resolution was insufficient to capture the dynamics of these fluctuations reliably, as seen previously in studies of transition paths at constant force [5,33]. We therefore remeasured the hairpin and reference constructs at non-constant force with high trap stiffness. Individual attempts at folding [Fig. 6(a), red] and unfolding [Fig. 6(a), orange], as well as transition paths [Fig. 6(a), blue] were identified as above. The distributions $p(x|NPF_F)$ and $p(x|NPF_U)$ were still asymmetric [Fig. 6(b)], but the effects of the beads and handles were more prominent [Figs. 6(c) and S6] owing to the reduction in the folding length change arising from compliance corrections [32]. Unfolding attempts could be reliably distinguished from bead and handle motions only for the largest fluctuations, those reaching

over 70%–80% of the way across the barrier region, and folding attempts could not be distinguished at all [Fig. 6(d)]. Within the restricted range where the fluctuations could be reliably identified as molecular, however, their dynamics could be probed.

Considering first the duration of fluctuations reaching at least 80% of the way across the barrier region [Fig. 6(e)], it differed from the distribution in Fig. 4(a) because the shortest-duration fluctuations were precluded by the requirement that all fluctuations have a minimum size. Expanding the distribution to include all fluctuations [Fig. 6(e), inset], we recovered the qualitatively expected shape but of course no longer excluding the many fluctuations arising purely from the beads and handles. The average duration of fluctuations reaching a given distance, $\tau(x_{\max})$, was more instructive [Fig. 6(f)] because it could be fit to Eq. (7) to determine D . Owing to the influence of the bead and handle fluctuations still being felt within much of this region, we restricted the fit to the six points furthest from x_1 . The fit [Fig. 6(f), dashed line] returned $D = 2.7 \pm 0.2 \times 10^5 \text{ nm}^2/\text{s}$, similar to the average value $2.4 \pm 0.2 \times 10^5 \text{ nm}^2/\text{s}$ obtained for this hairpin from analyses of different transition-path properties [6]. The observed average durations became progressively shorter than expected from this fit as x_{\max} moved closer to x_1 , the trend expected if the average were increasingly being biased by bead and handle fluctuations, which are faster.

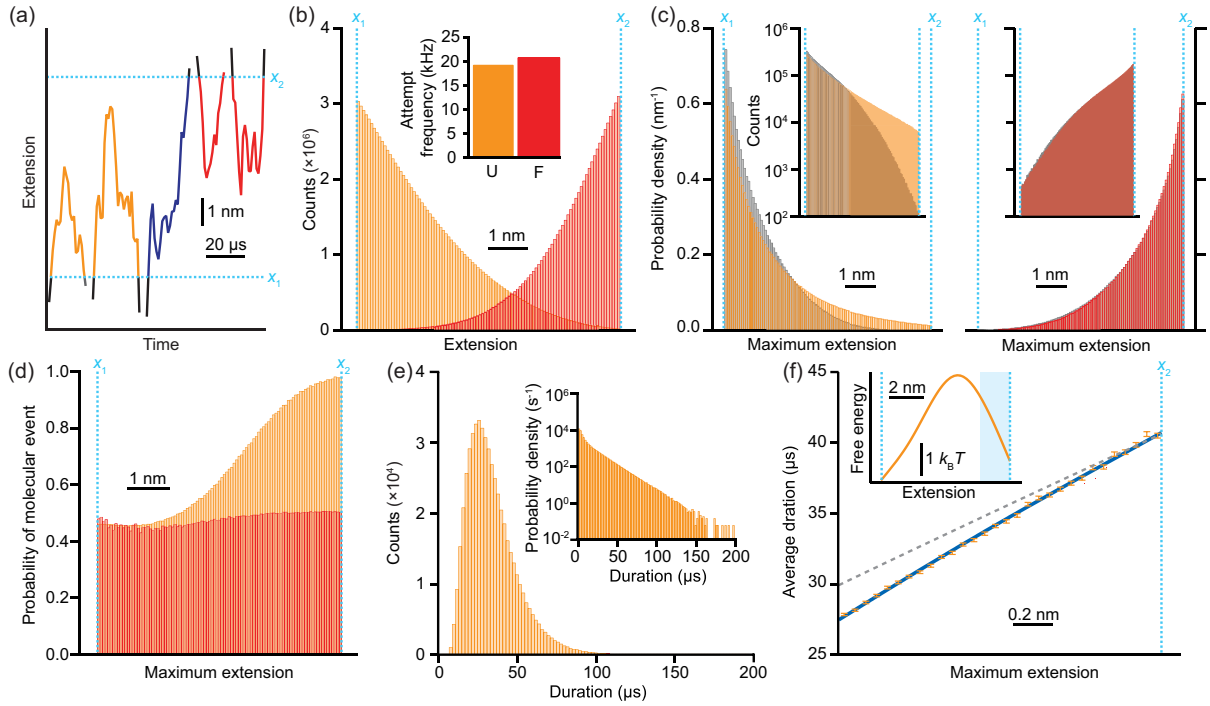


FIG. 6. Duration of nonproductive fluctuations in DNA hairpin folding. (a) Examples of folding attempts (red), unfolding attempts (orange), and a transition path (blue) from measurements at nonconstant force, where time resolution is higher. (b) Occupancy distributions for folding (red) and unfolding (orange) attempts. Inset: attempt frequencies. (c) Comparison of maximum extension distributions for folding (red) and unfolding (orange) to distributions for bead and handle fluctuations (gray), showing that only unfolding attempts can be distinguished. (d) Fraction of fluctuations associated with hairpin dynamics found by comparing the maximum extension distributions of the hairpin and reference constructs. (e) Durations of unfolding attempts reaching at least 80% of the way across the barrier. Inset: distribution of durations for all nonproductive unfolding fluctuations. (f) Average duration of unfolding attempts reaching at least 80% of the way across the barrier as a function of maximum extent. Dashed line: fit to Eq. (7) using six points closest to x_2 to minimize effects of bead and handle fluctuations. Solid line: fit including a second component from bead-handle fluctuations. Inset: barrier region of energy landscape for hairpin folding inferred from committer.

Treating the bead and handle fluctuations as a second population with higher D in a two-component fit to $\tau(x_{\max})$, where the relative population occupancies of molecular vs bead and handle fluctuations were given by Fig. 6(d), we found excellent agreement across the whole region being analyzed [Fig. 6(f), cyan]; the value of D for the hairpin was unchanged in this fit, and the value for bead and handle fluctuations ($D = 4.8 \pm 0.1 \times 10^5 \text{ nm}^2/\text{s}$) also matched previous results [34].

III. DISCUSSION

The basic framework for describing the thermally activated barrier crossing proposed by Arrhenius—the notion that the rate is given by a prefactor (k_0 , often interpreted as a basal attempt frequency) that is suppressed exponentially by the barrier height (ΔG^\ddagger) according to the relation $k = k_0 \exp(-\beta\Delta G^\ddagger)$ —has remained at the core of kinetic theories for over 130 years. However, the nonproductive fluctuations reflecting the vast majority of attempts at barrier crossing have been all but ignored experimentally to date. Our work shows that with sufficient

resolution in time and space along the reaction coordinate, it is possible to detect individual unsuccessful attempts at barrier crossing even in complex reactions like biomolecular folding. Furthermore, we provide a theoretical framework for analyzing the properties of nonproductive fluctuations. Such measurements and analyses allow access to the full dynamics within the barrier region, exploring a wider region of the energy landscape than in transition paths alone and yielding fundamental descriptors of the dynamics in these new regions, such as the diffusion coefficient.

One issue illuminated by these measurements is the meaning of the exponential prefactor in kinetic theories. This prefactor is often described as an “attempt frequency” for barrier crossing. Whereas such an interpretation is valid in the context of transition state theory, where the prefactor is equal to the number of reaction attempts per unit time, it is not so for the Kramers’ theory prefactor, which, despite its units of inverse time, cannot be interpreted as an attempt rate. In the case of the bead-hopping measurements described above, for example, the Kramers prefactor [given by $\beta D(\kappa_w \kappa_b)^{1/2}/2\pi$, where κ_w and κ_b are the stiffness of the

potential well and barrier, respectively] is $40 \pm 2 \text{ s}^{-1}$ for the forward reaction and $42 \pm 2 \text{ s}^{-1}$ for the reverse reaction. These prefactor rates are orders of magnitude smaller than the attempt frequencies observed experimentally: $1278 \pm 4 \text{ s}^{-1}$ (forward) and $1280 \pm 5 \text{ s}^{-1}$ (reverse), which themselves represent an underestimate owing to resolution limitations [23]. In contrast, the rates for productive barrier crossings (i.e., transition paths) predicted by Kramers' theory ($2.8 \pm 0.2 \text{ s}^{-1}$ forward, $4.9 \pm 0.2 \text{ s}^{-1}$ reverse) agree well with those observed experimentally ($3.3 \pm 0.2 \text{ s}^{-1}$ forward, $5.6 \pm 0.4 \text{ s}^{-1}$ reverse). This comparison highlights the sometimes overlooked point that Kramers' rate predictions should not be interpreted as an attempt frequency prefactor suppressed by an exponential barrier height term, as the Kramers' prefactor also incorporates effects like diffusive barrier recrossing. On the other hand, the experimentally observed attempt rates are defined by how often the boundaries defining the transition region—rather than the barrier—are crossed; since the vast majority of reaction attempts reach only a small distance into the barrier region, the observed attempt rates will depend most strongly on the boundary positions and the shape of the energy landscape nearby.

We found very close agreement between experiment and theory for the properties of nonproductive fluctuations in simple bead-hopping dynamics, as would be expected for an ideal model system. The comparison of experiment to theory was more difficult for the nonproductive attempts at hairpin unfolding and refolding, however, because of the artifacts introduced by the dynamics of the beads and handles used to apply force to the hairpin. We were nevertheless able to isolate parts of the barrier region where molecular fluctuations could be reliably identified. Ideally, to best distinguish molecular fluctuations from bead and handle fluctuations, the latter should have a distribution that is narrow compared to the width of the barrier region, achieved by maximizing the stiffness of the handles and beads while minimizing compliance corrections for the unfolding distance; in concert, the bead size should be minimized to maximize the time resolution of the measurement [35]. However, some of these requirements may conflict (e.g., small beads are less stiff, and higher trap stiffness can induce larger compliance corrections), leading to the need for technical compromises.

The analysis of nonproductive fluctuations presented here could, in principle, be extended to include other properties that have been analyzed for transition paths, such as local velocity distributions and average fluctuation shapes [6,8]. Pauses in the fluctuations could be analyzed to detect and characterize ubiquitous micro-wells within the barrier region [10] or more persistent kinetically trapped states, such as those that can occur in protein misfolding [12–14]. One property that could be particularly interesting is the diffusivity (position-dependent diffusion coefficient) $D(x)$, which reflects local roughness in the energy

landscape. Diffusivity is expected to be constant in reactions like bead hopping over a smooth landscape, but it is known to vary in more complex reactions such as folding [36,37], although the position dependence is difficult to measure [38]. Transition-path pauses provide one avenue to access $D(x)$ [10], but nonproductive fluctuations should provide another: Because these fluctuations can be classified by their maximum extent (unlike transition paths), incremental changes in $\tau(x_{\max})$ can be analyzed as x_{\max} changes to detect variations in D . Most importantly, such an analysis could report $D(x)$ for regions of the landscape that are not visited in transition paths and would be especially meaningful in cases like protein misfolding, given that diffusion can be much slower for misfolding than native folding [39] and hence $D(x)$ may be depressed in regions of the landscape featuring notable amounts of misfolding.

IV. CONCLUSION

We demonstrated direct measurements of nonproductive attempts at thermally driven barrier crossing, both in a model system of diffusive bead hopping and in a more complex system of biomolecular folding. We also developed tools for analyzing these nonproductive fluctuations, quantifying properties such as their occupancy, maximum extent, and duration in ways that characterize fundamental descriptors of the dynamics such as the diffusion coefficient. This work provides a comprehensive approach for detecting and characterizing nonproductive attempts at barrier crossing, offering a more complete picture of barrier-crossing dynamics.

V. METHODS

A. Bead-hopping measurements

Two optical traps were created from a 1064-nm diode-pumped solid-state laser by separating the beam into independent polarizations. The positions and intensities of each trap beam were controlled independently by acousto-optic deflectors to generate potential wells separated by 234 nm. A single 820-nm diameter polystyrene bead was held in the traps, and its position was monitored from laser light scattered onto quadrant photodiodes (First Sensor). Data were sampled at 1 MHz and filtered online at the Nyquist frequency with an 8-pole Bessel filter. A total of 145 s of hopping was measured. Data were collected with Labview 2018 software. The trap stiffnesses, measured from the variance of the bead position and the roll-off frequency of the noise power spectral density [40], were $0.0053 \pm 0.0002 \text{ pN/nm}$ for the left well and $0.0051 \pm 0.0002 \text{ pN/nm}$ for the right well.

B. Analysis of bead hopping

The energy landscape for bead hopping, found from an inverse Boltzmann transform of the bead-position

probability distribution $p(x)$ with a bin size of 0.31 nm, was used to define the boundaries of the barrier region as the middle 2/3 of the distance between the well centers. Individual transition paths and nonproductive fluctuations were isolated from the trajectories by extracting the segments lying within the barrier region, as well as the points immediately following or preceding those in the barrier region; segments whose start and end points were on the same side of the barrier region were classified as nonproductive fluctuations, whereas segments whose start and end points were on opposite sides were classified as transition paths.

Occupancy distributions for nonproductive fluctuations were calculated directly from the isolated segments of the trajectories. The maximum extension reached into the transition region during unsuccessful attempts was found by detecting the lowest (highest) x value reached within the barrier region for each forward (reverse) crossing attempt. The duration of each transition path and nonproductive fluctuation was found from the trajectories by measuring the length of time spent within the barrier region; when the barrier boundary was crossed between sampling points, the crossing time was calculated by linear interpolation between the points straddling the boundary.

Fitting of $p(x_{\max}|\text{NPF}_{\text{F/R}})$ to Eq. (5) was done while dividing by a constant to act as a normalization factor. To account for artifacts near the proximal boundary (x_1 or x_2), we omitted the points nearest the boundary from the fitting until the fit passed a χ^2 test as well as a Kolmogorov-Smirnov test for residual normality, both at the 95% confidence level (Fig. S2 in Ref. [11]); the four points closest to x_2 were omitted for the forward reaction, whereas the seven points closest to x_1 were omitted for the reverse reaction. When fitting $\tau(x_{\max})$ to Eq. (7), we followed the same procedure of omitting the points nearest the boundary until the fit passed both the χ^2 and Kolmogorov-Smirnov tests (Fig. S3 in Ref. [11]); here, the five points closest to x_2 were omitted for the forward reaction, whereas the three points closest to x_1 were omitted for the reverse reaction. To account for any uncertainty introduced during this process, the error in D was estimated as the average difference between the values obtained as above and the values obtained by omitting either two or seven points closest to the originating boundary, representing the range of point omissions required for one of the two tests to pass in all fits. All fits were performed in MATLAB 2021A using the trust region reflective method.

C. Hairpin fluctuation measurements

Samples containing DNA hairpin 30R50/T4 from Ref. [28] connected to double-stranded (ds) DNA were prepared as described previously [10]. Briefly, a DNA oligomer containing the hairpin sequence separated by abasic sites from a 5' ligation overhang and a 3' primer sequence was used to generate an 801-bp dsDNA handle

with the hairpin attached to one end via autosticky polymerase chain reaction (PCR). This PCR product was then ligated via the 5' overhang to a 1260-bp dsDNA handle with a complementary overhang. The resulting product was incubated at about 100 pM concentration to 600- and 820-nm diameter polystyrene beads (about 250 pM), which bound to the hairpin construct via biotin:avidin and digoxigenin:anti-digoxigenin pairs to produce “dumbbells” for trapping. Dumbbells diluted to about 500 fM in 50 mM MOPS, pH 7.0, with 200 mM KCl and an oxygen scavenging system (8 mU/ μ L glucose oxidase, 20 mU/ μ L catalase, 0.01% w/v D-glucose) were inserted into a sample cell for trapping.

Hairpins were measured in a dual-beam optical trap described previously [10]. Constant-force measurements were done using a passive force clamp [32], adjusting the power of the zero-stiffness trap holding the 600-nm bead until the hairpin spent approximately equal amounts of time in the folded and unfolded states. Data were sampled at 1 MHz and filtered online at the Nyquist frequency with an eight-pole Bessel filter, with the nonzero trap stiffness set to about 0.4 pN/nm. Constant-force trajectories lasting a total of 106 s were measured from four hairpin molecules. Trajectories at nonconstant force were measured by setting the trap stiffnesses to about 1.0 and 0.6 pN/nm, and then moving the traps apart until the hairpin fluctuated between folded and unfolded states at roughly equal rates. Data were sampled and filtered as above. Nonconstant force trajectories lasting a total of 758 s were measured from seven hairpin molecules.

To measure the effect of handle and bead fluctuations, reference constructs consisting of the dsDNA handles and single-stranded linker regions (but lacking the hairpin) were prepared, similar to the hairpin constructs. The reference construct was measured identically to the hairpin under constant-force and nonconstant-force conditions. For comparison to constant-force measurements, the reference construct was held at the unfolding force of the hairpin, $F_{1/2} = 13.9 \pm 0.2$ pN [28]; trajectories lasting a total of 158 s were measured from four molecules. For comparison to nonconstant-force measurements, the reference construct was measured at two forces to mimic the different forces experienced by the hairpin under these conditions: the force in the folded state, $F_{\text{F}} = 16.1 \pm 0.2$ pN (trajectories lasting a total of 140 s from three molecules), and the force in the unfolded state, $F_{\text{U}} = 11.1 \pm 0.2$ pN (trajectories lasting a total of 88 s from three molecules).

The instrument response time under the conditions used for high-stiffness measurements of hairpin 30R50/T4 has been characterized previously, via (1) the relaxation time of the reference (handle-only) construct after abruptly changing the distance between the traps, yielding 6 ± 1 μ s for jumps equivalent to the extension change for hairpin unfolding [5]; and (2) the decay constants for the auto-correlation function [34] and power spectral density [5]

calculated from extension fluctuations within the wells, both around 9 μs . The relaxation time approach is the most directly related to the measurement. Noting that, when responding to a change in extension, the beads will move to their new position faster when the distance change is smaller (an issue relevant to nonproductive fluctuations because of their variable length), we estimated the response time for fluctuations of different size by dividing the relaxation time by the extension change, finding about 0.4 $\mu\text{s}/\text{nm}$. For constant-force measurements of hairpin 30R50/T4, the response time was previously characterized via the autocorrelation decay time [34] to be around 40 μs , roughly 4–5 times slower than in the nonconstant-force measurements.

D. Analysis of hairpin folding

The barrier region was defined exactly as for the bead-hopping experiments, and the transition paths and nonproductive fluctuations were also identified as above, using the end-to-end extension of the molecule (instead of the bead position) as the reaction coordinate. In order to obtain good statistics for the rare fluctuations reaching far into the barrier region, the trajectories from all molecules measured under a given condition (constant force or high stiffness) were pooled together for analysis; to account for minor differences in length calibration between molecules, the extension values for each molecule were scaled so that the unfolding distance of each hairpin matched the average value.

Hairpin data were analyzed similarly to bead-hopping data. Because handle/bead fluctuations affect the extension probability distribution, the energy landscape for hairpin folding was found using committor reconstruction [31] rather than inverting the Boltzmann distribution. This method provides a reasonable approximation for this hairpin even though it is not strictly correct [41]. Briefly, $\Phi_{\text{R}}(x)$ was calculated directly from the trajectory and the landscape derived from $\beta U(x) = \ln[-d\Phi_{\text{R}}(x)/dx]$; to reduce noise from numerical differentiation, a smoothing spline with a smoothing factor of 0.8 was applied to the result. To assess the fluctuations arising from beads/handles, mock measurements of the reference construct lacking hairpin were used. “Boundaries” mimicking x_1 and x_2 were placed at the same distance from the average reference extension as they were from the folded and unfolded states of the hairpin, respectively, and the handle/bead fluctuations mimicking nonproductive attempts were identified as for the hairpin data (Figs. S4 and S6). The probability distribution that the observed fluctuations reaching a certain distance were due to hairpin motions was calculated by dividing the maximum extension distribution of the hairpin by the sum of the maximum extension distributions of the hairpin and handle construct.

All fits were performed in MATLAB 2021A using the trust region reflective algorithm. To estimate the effect

of the handle/bead fluctuations on $\tau(x_{\text{max}})$, we modified Eq. (7) to include a component from motions of the handles/beads as well as the hairpin, replacing the constant D with a position-dependent version $D(x_{\text{max}}) = D_{\text{HB}} + p_{\text{hp}}(x_{\text{max}})[D_{\text{hp}} - D_{\text{HB}}]$, where D_{hp} is the diffusion coefficient for the hairpin, D_{HB} is the handle/bead diffusion coefficient, and $p_{\text{hp}}(x_{\text{max}})$ is the probability that fluctuations reaching a maximum extension x_{max} arose from hairpin dynamics. To estimate the error on D from the hairpin data, an uncertainty of about $1 k_{\text{B}}T$ was assumed for the barrier height based on previous work [31], and the data were refit in a bootstrapping analysis while scaling the energy landscape by the resampled barrier height, taking the standard deviation from 500 resamplings as the error in D .

Data supporting the findings in this work have been deposited in Figshare [42].

ACKNOWLEDGMENTS

This work was supported by the Natural Sciences and Engineering Research Council (grant reference number RGPIN-2018-04673) and the National Research Council Canada.

M. T. W. and A. L. designed the research; A. L. and N. Q. H. provided reagents; A. L., A. D., and N. Q. H. measured the data; A. L. and A. D. analyzed the data; M. T. W. and A. L. wrote the manuscript; all authors edited the manuscript.

The authors declare no competing interests.

-
- [1] P. Hänggi, P. Talkner, and M. Borkovec, *Reaction-rate theory: Fifty years after Kramers*, *Rev. Mod. Phys.* **62**, 251 (1990).
 - [2] P. G. Bolhuis, D. Chandler, C. Dellago, and P. L. Geissler, *Transition path sampling: Throwing ropes over rough mountain passes, in the dark*, *Annu. Rev. Phys. Chem.* **53**, 291 (2002).
 - [3] N. Q. Hoffer and M. T. Woodside, *Probing microscopic conformational dynamics in folding reactions by measuring transition paths*, *Curr. Opin. Chem. Biol.* **53**, 68 (2019).
 - [4] H. S. Chung, K. McHale, J. M. Louis, and W. A. Eaton, *Single-molecule fluorescence experiments determine protein folding transition path times*, *Science* **335**, 981 (2012).
 - [5] K. Neupane, D. A. N. Foster, D. R. Dee, H. Yu, F. Wang, and M. T. Woodside, *Direct observation of transition paths during the folding of proteins and nucleic acids*, *Science* **352**, 239 (2016).
 - [6] K. Neupane, N. Q. Hoffer, and M. T. Woodside, *Measuring the local velocity along transition paths during the folding of single biological molecules*, *Phys. Rev. Lett.* **121**, 018102 (2018).
 - [7] F. Sturzenegger, F. Zosel, E. D. Holmstrom, K. J. Buholzer, D. E. Makarov, D. Nettels, and B. Schuler, *Transition path*

- times of coupled folding and binding reveal the formation of an encounter complex, *Nat. Commun.* **9**, 4708 (2018).
- [8] N. Q. Hoffer, K. Neupane, A. G. T. Pyo, and M. T. Woodside, *Measuring the average shape of transition paths during the folding of a single biological molecule*, *Proc. Natl. Acad. Sci. U.S.A.* **116**, 8125 (2019).
- [9] J.-Y. Kim and H. S. Chung, *Disordered proteins follow diverse transition paths as they fold and bind to a partner*, *Science* **368**, 1253 (2020).
- [10] N. Q. Hoffer, K. Neupane, and M. T. Woodside, *Observing the base-by-base search for native structure along transition paths during the folding of single nucleic acid hairpins*, *Proc. Natl. Acad. Sci. U.S.A.* **118**, e2101006118 (2021).
- [11] See Supplemental Material at <http://link.aps.org/supplemental/10.1103/PhysRevX.14.011017> for Figures S1–S6.
- [12] J. Stigler, F. Ziegler, A. Gieseke, J. C. M. Gebhardt, and M. Rief, *The complex folding network of single calmodulin molecules*, *Science* **334**, 512 (2011).
- [13] H. Yu, X. Liu, K. Neupane, A. N. Gupta, A. M. Brigley, A. Solanki, I. Sosova, and M. T. Woodside, *Direct observation of multiple misfolding pathways in a single prion protein molecule*, *Proc. Natl. Acad. Sci. U.S.A.* **109**, 5283 (2012).
- [14] R. Tapia-Rojo, M. Mora, S. Board, J. Walker, R. Boujemaa-Paterski, O. Medalia, and S. Garcia-Manyes, *Enhanced statistical sampling reveals microscopic complexity in the talin mechanosensor folding energy landscape*, *Nat. Phys.* **19**, 52 (2023).
- [15] F. Chiti and C. M. Dobson, *Protein misfolding, functional amyloid, and human disease*, *Annu. Rev. Biochem.* **75**, 333 (2006).
- [16] L. I. McCann, M. Dykman, and B. Golding, *Thermally activated transitions in a bistable three-dimensional optical trap*, *Nature (London)* **402**, 785 (1999).
- [17] N. Zijlstra, D. Nettelts, R. Satija, D. E. Makarov, and B. Schuler, *Transition path dynamics of a dielectric particle in a bistable optical trap*, *Phys. Rev. Lett.* **125**, 146001 (2020).
- [18] M. T. Woodside, P. C. Anthony, W. M. Behnke-Parks, K. Larizadeh, D. Herschlag, and S. M. Block, *Direct measurement of the full, sequence-dependent folding landscape of a nucleic acid*, *Science* **314**, 1001 (2006).
- [19] G. Hummer, *From transition paths to transition states and rate coefficients*, *J. Chem. Phys.* **120**, 516 (2003).
- [20] K. Neupane, A. P. Manuel, J. Lambert, and M. T. Woodside, *Transition-path probability as a test of reaction-coordinate quality reveals DNA hairpin folding is a one-dimensional diffusive process*, *J. Phys. Chem. Lett.* **6**, 1005 (2015).
- [21] K. Neupane, A. P. Manuel, and M. T. Woodside, *Protein folding trajectories can be described quantitatively by one-dimensional diffusion over measured energy landscapes*, *Nat. Phys.* **12**, 700 (2016).
- [22] A. M. Berezhkovskii and D. E. Makarov, *Communication: Transition-path velocity as an experimental measure of barrier crossing dynamics*, *J. Chem. Phys.* **148**, 201102 (2018).
- [23] D. E. Makarov, A. Berezhkovskii, G. Haran, and E. Pollak, *The effect of time resolution on apparent transition path times observed in single-molecule studies of biomolecules*, *J. Phys. Chem. B* **126**, 7966 (2022).
- [24] R. Huang, I. Chavez, K. M. Taute, B. Lukić, S. Jeney, M. G. Raizen, and E.-L. Florin, *Direct observation of the full transition from ballistic to diffusive Brownian motion in a liquid*, *Nat. Phys.* **7**, 576 (2011).
- [25] S. Chaudhury and D. E. Makarov, *A harmonic transition state approximation for the duration of reactive events in complex molecular rearrangements*, *J. Chem. Phys.* **133**, 034118 (2010).
- [26] A. G. Baker, C.-Y. Chuang, M. Whitmore, and M. J. Comstock, *Randomizing phase to remove acousto-optic device wobble errors for high-resolution optical tweezers*, *Appl. Opt.* **57**, 1752 (2018).
- [27] R. Zwanzig, *Diffusion in a rough potential*, *Proc. Natl. Acad. Sci. U.S.A.* **85**, 2029 (1988).
- [28] M. T. Woodside, W. M. Behnke-Parks, K. Larizadeh, K. Travers, D. Herschlag, and S. M. Block, *Nanomechanical measurements of the sequence-dependent folding landscapes of single nucleic acid hairpins*, *Proc. Natl. Acad. Sci. U.S.A.* **103**, 6190 (2006).
- [29] A. N. Gupta, A. Vincent, K. Neupane, H. Yu, F. Wang, and M. T. Woodside, *Experimental validation of free-energy-landscape reconstruction from non-equilibrium single-molecule force spectroscopy measurements*, *Nat. Phys.* **7**, 631 (2011).
- [30] M. C. Engel, D. B. Ritchie, D. A. N. Foster, K. S. D. Beach, and M. T. Woodside, *Reconstructing folding energy landscape profiles from nonequilibrium pulling curves with an inverse Weierstrass integral transform*, *Phys. Rev. Lett.* **113**, 238104 (2014).
- [31] A. P. Manuel, J. Lambert, and M. T. Woodside, *Reconstructing folding energy landscapes from splitting probability analysis of single-molecule trajectories*, *Proc. Natl. Acad. Sci. U.S.A.* **112**, 7183 (2015).
- [32] W. J. Greenleaf, M. T. Woodside, E. A. Abbondanzieri, and S. M. Block, *Passive all-optical force clamp for high-resolution laser trapping*, *Phys. Rev. Lett.* **95**, 208102 (2005).
- [33] K. Neupane, D. B. Ritchie, H. Yu, D. A. N. Foster, F. Wang, and M. T. Woodside, *Transition path times for nucleic acid folding determined from energy-landscape analysis of single-molecule trajectories*, *Phys. Rev. Lett.* **109**, 068102 (2012).
- [34] K. Neupane and M. T. Woodside, *Quantifying instrumental artifacts in folding kinetics measured by single-molecule force spectroscopy*, *Biophys. J.* **111**, 283 (2016).
- [35] A. Devi, K. Neupane, H. Jung, K. C. Neuman, and M. T. Woodside, *Non-linear effects in optical trapping of titanium dioxide and diamond nanoparticles*, *Biophys. J.* **122**, 3439 (2023).
- [36] R. B. Best and G. Hummer, *Coordinate-dependent diffusion in protein folding*, *Proc. Natl. Acad. Sci. U.S.A.* **107**, 1088 (2010).
- [37] J. Chahine, R. J. Oliveira, V. B. P. Leite, and J. Wang, *Configuration-dependent diffusion can shift the kinetic transition state and barrier height of protein folding*, *Proc. Natl. Acad. Sci. U.S.A.* **104**, 14646 (2007).
- [38] D. A. N. Foster, R. Petrosyan, A. G. T. Pyo, A. Hoffmann, F. Wang, and M. T. Woodside, *Probing position-dependent diffusion in folding reactions using single-molecule force spectroscopy*, *Biophys. J.* **114**, 1657 (2018).
- [39] H. Yu, D. R. Dee, X. Liu, A. M. Brigley, I. Sosova, and M. T. Woodside, *Protein misfolding occurs by slow*

- diffusion across multiple barriers in a rough energy landscape*, *Proc. Natl. Acad. Sci. U.S.A.* **112**, 8308 (2015).
- [40] K. C. Neuman and S. M. Block, *Optical trapping*, *Rev. Sci. Instrum.* **75**, 2787 (2004).
- [41] R. Covino, M. T. Woodside, G. Hummer, A. Szabo, and P. Cossio, *Molecular free energy profiles from force spectroscopy experiments by inversion of observed committors*, *J. Chem. Phys.* **151**, 154115 (2019).
- [42] A. Lyons, A. Devi, N. Q. Hoffer, and M. T. Woodside, *Trajectories of non-productive attempts at thermally activated energy-barrier crossing for beads and DNA hairpin 30R50/T4*, Figshare (2023), [10.6084/m9.figshare.24794955](https://doi.org/10.6084/m9.figshare.24794955).